

Signal to noise ratio of upgraded imaging bolometer for KSTAR

Cite as: Rev. Sci. Instrum. **89**, 10E115 (2018); <https://doi.org/10.1063/1.5038935>

Submitted: 07 May 2018 • Accepted: 11 June 2018 • Published Online: 10 October 2018

Byron J. Peterson,  Seungtae Oh, Dongcheol Seo, et al.

COLLECTIONS

Paper published as part of the special topic on [Proceedings of the 22nd Topical Conference on High-Temperature Plasma Diagnostics](#)



View Online



Export Citation



CrossMark

ARTICLES YOU MAY BE INTERESTED IN

[Reconstruction of radiation profiles near the plasma boundary using an infrared imaging video bolometer in KSTAR](#)

Review of Scientific Instruments **89**, 10E111 (2018); <https://doi.org/10.1063/1.5038904>

[Forward projection matrix derivation through Monte-Carlo ray-tracing of KSTAR infra-red imaging video bolometer \(IRVB\)](#)

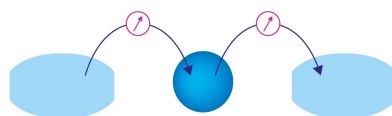
Review of Scientific Instruments **89**, 10E118 (2018); <https://doi.org/10.1063/1.5036929>

[Experimental tests of an infrared video bolometer on Alcator C-Mod](#)

Review of Scientific Instruments **89**, 103507 (2018); <https://doi.org/10.1063/1.5047050>

Webinar

Interfaces: how they make
or break a nanodevice



March 29th – Register now



Zurich
Instruments

Signal to noise ratio of upgraded imaging bolometer for KSTAR

Byron J. Peterson,^{1,2,a)} Seungtae Oh,³ Dongcheol Seo,³ Juhyeok Jang,⁴ Jae Sun Park,⁴ Kiyofumi Mukai,^{1,2} and Wonho Choe^{4,5}

¹National Institute for Fusion Science, Toki, Japan

²SOKENDAI, The Graduate University for Advanced Studies, Toki, Japan

³National Fusion Research Institute, Daejeon, South Korea

⁴Department of Physics, Korea Advanced Institute of Science and Technology, Daejeon, South Korea

⁵Department of Nuclear and Quantum Engineering, Korea Advanced Institute of Science and Technology, Daejeon, South Korea

(Presented 16 April 2018; received 7 May 2018; accepted 11 June 2018;
published online 10 October 2018)

An InfraRed imaging Video Bolometer (IRVB) was installed on KSTAR in 2012 having a $\sim 2 \mu\text{m} \times 7 \text{ cm} \times 9 \text{ cm}$ Pt foil blackened with graphite and a $5 \text{ mm} \times 5 \text{ mm}$ aperture located 7.65 cm from the foil with 16×12 channels and a time resolution of 10 ms. The IR camera was an Indigo Phoenix (InSb, 320×256 pixels, 435 fps, $<25 \text{ mK}$). In 2017, the IRVB was upgraded by replacing the IR camera with a FLIR SC7600 (InSb, 640×512 pixels, 105 fps, $<25 \text{ mK}$). The aperture area was reduced by approximately half to $3.5 \text{ mm} \times 3.5 \text{ mm}$, and the number of channels was quadrupled to 32×24 . A synthetic image derived using the projection matrix for the upgraded IRVB from a Scrape Off Layer Plasma Simulator (SOLPS) model with 146 kW of total radiated power had a maximum signal of 7.6 W/m^2 and a signal to noise ratio (SNR) of 11. Experimental data for a plasma with parameters similar to the SOLPS model (total radiated power of 158 kW) had a maximum signal of 12.6 W/m^2 and noise equivalent power density (SNR) of 0.9 W/m^2 (14). *Published by AIP Publishing.*
<https://doi.org/10.1063/1.5038935>

I. INFRA-RED IMAGING VIDEO BOLOMETER

Bolometric measurements are essential to the estimation of the total radiated power from a magnetic fusion device for the purposes of power balance¹ and impurity seeding studies.² Conventional bolometer detectors to be installed in ITER are based on the temperature dependence of the electrical resistance of a metal meander which is thermally coupled to a photon absorbing foil by an intermediate insulating substrate.³ Using a Wheatstone bridge and associated electronic circuitry to sense the change in the resistance resulting from the heat imparted on the foil by the absorbed photon, the resistive bolometer is susceptible to electromagnetic noise from various sources which are abundant in a fusion device, in particular from ion cyclotron resonant frequency induced noise.⁴ In addition, the insulating layer which is needed to electrically isolate the absorbing foil from the sensing meander presents challenges in constructing a resistive bolometer that can survive the extreme temperature swings and nuclear radiation of a fusion reactor.⁵ The resistive bolometers are typically arranged in linear arrays behind a collimating aperture to provide line integrated measurements of radiation from different parts of the plasma. With a sufficient number of detectors arrayed around the plasma, a tomographic inversion can be performed to provide a local measurement of the plasma emissivity.⁶

In an effort to develop a more reactor-relevant bolometer by avoiding the problems of the resistive bolometers with electromagnetic noise and large temperature variations, a new type of bolometer known as the InfraRed imaging Video bolometer (IRVB)⁷ has been under development,⁸ which leverages off the advances in infrared (IR) imaging technology to measure the temperature change in a foil absorbing radiation from the plasma. By using a graphite blackened foil, the broadband radiation absorbed through a collimating aperture is efficiently converted into IR radiation that can be transferred nearly noiselessly by appropriate IR optics to an IR camera outside of the vacuum vessel. By dispensing with the substrate and resistive meander, this avoids the previously mentioned problems characteristic of the resistive bolometer, while bringing the power of imaging to bolometric measurement.

In this paper, we look at one of the first applications of this diagnostic to a tokamak in terms of sensitivity, as quantified by the signal and noise levels, obtained through estimation, modeling, and experiment. In Sec. II, the upgrade will be described. In Sec. III, the equations and parameters used in the noise and rough signal estimation will be introduced. In Sec. IV, the Scrape Off Layer Plasma Simulator (SOLPS) model will be introduced, the calculation of the response matrix will be explained, and the resulting signal levels from synthetic images will be shown. In Sec. V, experimental images from the upgraded IRVB will be shown and compared with synthetic images, and the resulting signal and noise levels from the original and upgraded IRVBs will be compared. In Sec. VI, the results of the comparison will be discussed to give a perspective on future applications of the IRVB.

Note: Paper published as part of the Proceedings of the 22nd Topical Conference on High-Temperature Plasma Diagnostics, San Diego, California, April 2018.

^{a)}Author to whom correspondence should be addressed: peterson@LHD.nifs.ac.jp.

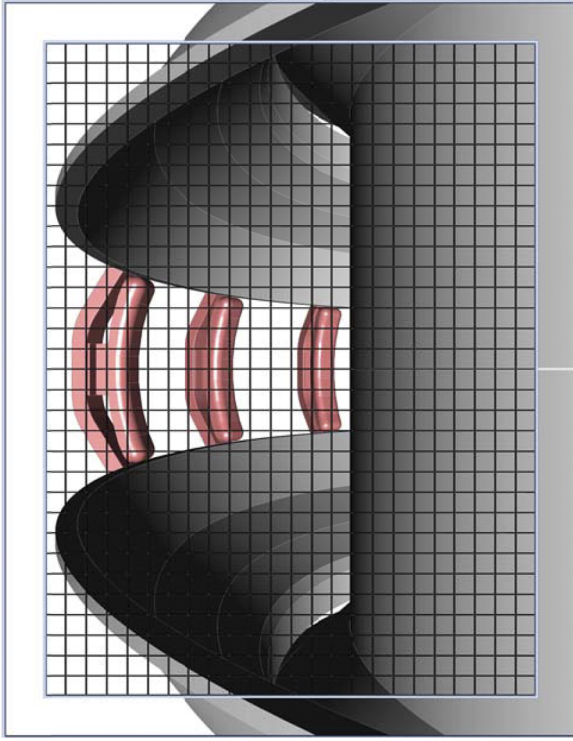


FIG. 1. Field of view of IRVB on KSTAR. The outer rectangle shows the edge of the frame and the grid shows bolometer pixels.

II. IRVB UPGRADE FOR KSTAR

In 2011, a $\sim 2 \mu\text{m}$ thick $\times 7 \text{ cm}$ (horizontal) $\times 9 \text{ cm}$ (vertical) Pt foil, mounted in a copper frame and blackened with graphite spray, was installed in a pinhole camera having an aperture of area, A_{ap} , of $5 \text{ mm} \times 5 \text{ mm}$ square, located a distance, l_{ap-f} , 7.65 cm in front of the foil. The foil has a tangential view through the aperture of the entire plasma cross-section as shown in Fig. 1. The side of the foil opposite to the plasma facing surface could be viewed from outside the vacuum vessel through a 10 cm diameter CaF_2 vacuum window. In 2012, the Phoenix IR camera and IR optics previously used on JT-60U⁹ were installed to view the foil. In 2016, the IR camera was replaced with a FLIR SC7600 IR camera. The major differences were an increase in the number of pixels from 256×320 to 512×640 and a reduction in the full-frame frame rate, f_{IR} , from 345 f/s to 105 f/s . Also the bolometer camera aperture size was reduced to $3.5 \text{ mm} \times 3.5 \text{ mm}$. Since the InSb focal plane array dimensions were the same, the optics could be utilized without any changes. This resulted

in an increase of the bolometer pixels from 12×16 to 24×32 . By utilizing the central $6 \text{ cm} \times 8 \text{ cm}$ portion of the foil, this gives a bolometer pixel area, A_{bol} , of $2.5 \text{ mm} \times 2.5 \text{ mm}$. The aperture linear dimension is 1.4 times that of the bolometer pixel, which recent tomographic modeling work has shown to be the maximum relative aperture size without degrading the tomographic reconstruction.¹⁰ The improvement in the spatial resolution of the tomographic reconstruction with the increase in the number of bolometer pixels has already been demonstrated through modeling.¹¹

III. ESTIMATION OF IRVB NOISE AND SIGNAL

The estimation of signal and noise used in this study has been previously used and documented.^{12,13} The noise equivalent power density, S_{IRVB} , which is a figure of merit for the sensitivity of the IRVB is given by Eq. (10) in Ref. 8 as

$$S_{IRVB} = \frac{\eta_{IRVB} N_{bol}}{A_f} = \frac{\sqrt{10} k t_f \sigma_{IR}}{\sqrt{f_{IR} N_{IR}}} \sqrt{\frac{N_{bol}^3 f_{bol}}{A_f^2} + \frac{N_{bol} f_{bol}^3}{5 \kappa^2}} \quad (1)$$

with $\sigma_{IR} = 15 \text{ mK}$, noise equivalent temperature (NET) of IR camera, η_{IRVB} , the noise equivalent power, N_{bol} , number of bolometer channels, $A_f = 48 \text{ cm}^2$, utilized area of the foil, $f_{bol} = 100 \text{ 1/s}$, effective frame rate of bolometer, N_{IR} , utilized number of IR camera pixels, $\kappa = 0.2506 \text{ cm}^2/\text{s}$, foil heat diffusivity, $k = 71.6 \text{ W/mK}$, foil heat conductivity, and $t_f = 2 \mu\text{m}$, foil thickness. The NET of the IR camera is conservatively estimated based on the 11.2 mK value that was obtained for JT-60U.⁹ The only difference between the JT-60U case and the KSTAR case is that a sapphire window was used on JT-60U, while a CaF_2 window was used on KSTAR, which has better transmission than the sapphire window. Therefore the assumption of 15 mK is conservative and justified. A rough estimate of the radiated power density, S_{signal} , is given by

$$S_{signal} = \frac{P_{signal}}{A_{bol}} = \frac{A_{bol} A_{ap} \cos^4 \theta P_{rad} l_{plasma}}{A_{bol} 4 \pi l_{ap-f}^2 V_{plasma}}, \quad (2)$$

where $\theta = 20^\circ$ is the average angle between the sight line and the foil normal vector, $l_{plasma} = 3 \text{ m}$, is the length of the sightline through the plasma and $P_{rad} = 146 \text{ kW}$ of the radiated power is assumed to be uniformly emanating from the $V_{plasma} = 15 \text{ m}^3$ volume plasma. This value of P_{rad} is chosen to match the value given by the SOLPS model in Sec. IV. Taking the ratio of Eq. (2) divided by Eq. (1) gives a signal to noise ratio (SNR) which is shown in Table I.

TABLE I. Signal and noise estimates for the original and upgraded IRVBs on KSTAR. Numbers in () are for the plasma with Krypton puffing in shot 16950 whose data are shown in Fig. 5.

IRVB	IRVB channel number	A_{ap} (mm^2)	S_{IRVB} (a) [Eq. (1)] (W/m^2)	S_{signal} (b) [Eq. (2)] (W/m^2)	SNR (b/a)	S_{signal} (c) (syn. data) (W/m^2)	SNR (c/a)	S_{IRVB} (d) (exp. data) (W/m^2)	S_{signal} (e) (exp. data) (W/m^2)	SNR (e/d)
Original	12×16	5×5	0.39	7.7	20
Upgrade	24×32	3.5×3.5	0.71	3.8	5.4	7.62	10.7	0.90 (2.1)	12.64 (115.3)	14.1 (54.9)

IV. SOLPS MODEL, RESPONSE MATRIX CALCULATION, AND SYNTHETIC IMAGES

In order to calculate the synthetic images, S_i , for channel number i , for the purpose of signal estimation, a projection

matrix, H_{ij} , where j is the plasma voxel index, is calculated and multiplied by the emissivity, I_j , from the SOLPS model,

$$S_i = \sum_j H_{ij} I_j. \quad (3)$$

The SOLPS model used in this work is the SOLPS-ITER code package¹⁴ and treats all the charge states of D (fuel) and C (impurity) ions. The SOLPS grid for KSTAR has 96 (poloidal) \times 36 (radial) cells in the edge and divertor regions. The input power is 250 kW each for both electrons and ions. The electron density at the outer mid-plane separatrix is $2.3 \times 10^{19} \text{ m}^{-3}$. The perpendicular heat diffusion coefficient for ions is set to $0.5 \text{ m}^2/\text{s}$ and $X_i = X_e = 1.0 \text{ m}^2/\text{s}$. The emissivity data from the model are first resampled onto a 5250 (R) \times 2900 (Z) grid having cell dimensions of $\Delta R = 0.2 \text{ mm}$ and $\Delta Z = 1 \text{ mm}$ in the range $1.26 \text{ m} < R < 2.31 \text{ m}$ and $-1.45 \text{ m} < Z < 1.45 \text{ m}$ to ensure that the cell size is smaller than the original cell size for accurate resampling. Then the data are resampled onto a grid having 21 (R) \times 58 (Z), 5 cm square cells in the same range as the previous grid, as shown in Fig. 2. Prior to resampling, the total radiated power was 147 kW. After resampling, it was slightly reduced to 146 kW.

The projection matrix was generated for the upgraded IRVB by stepping 1 cm (in the direction normal to the

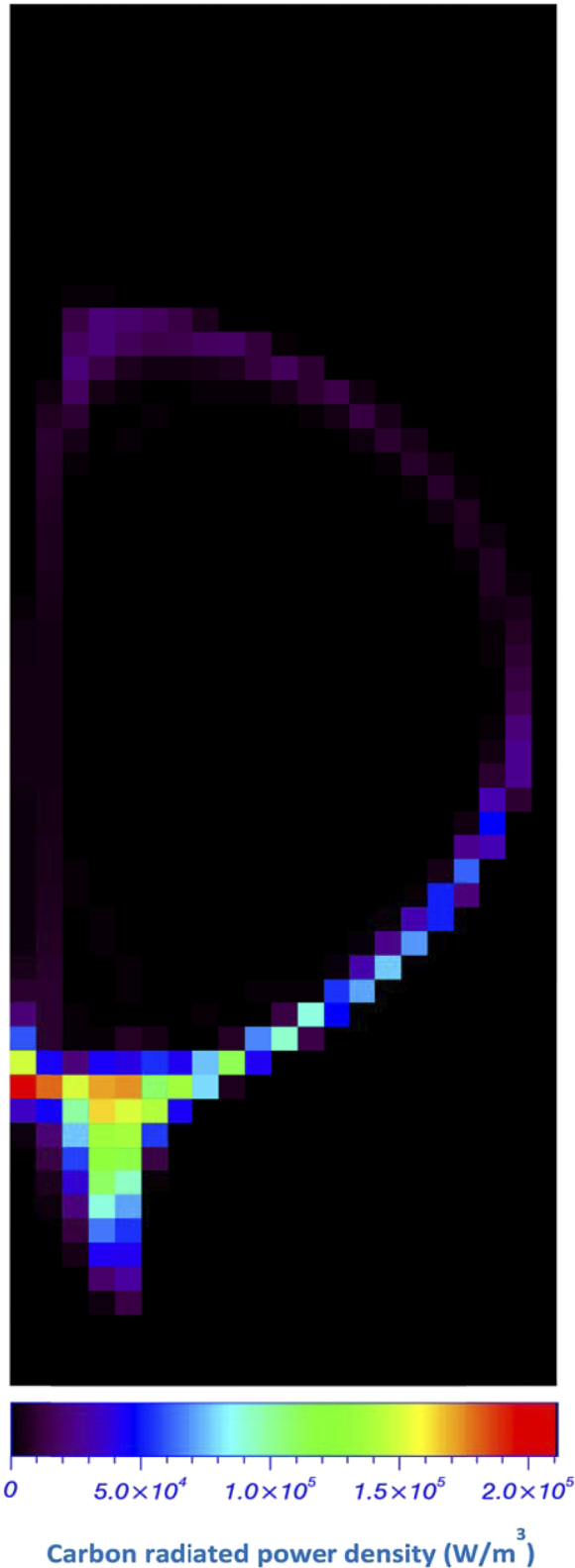


FIG. 2. Plasma emissivity profile from SOLPS after resampling to a 5 cm grid.

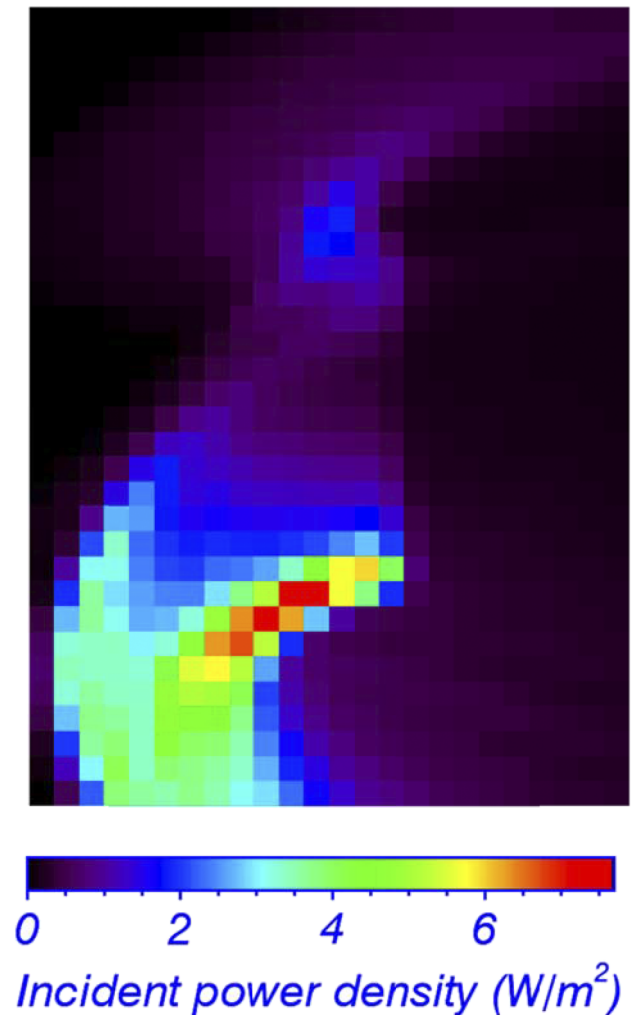


FIG. 3. Synthetic image from SOLPS data.

foil) along the line of sight until the wall was encountered. The aperture was subdivided to keep the dimensions of the subapertures below 1 cm. The bolometer pixel was not subdivided. The dimensions of the projection matrix were then 768 (i , bolometer pixels) \times 1218 (j , plasma voxels).

The synthetic image resulting from the vector multiplication of the response matrix by the emissivity matrix is shown in Fig. 3. The maximum signal level and the corresponding SNR are shown in Table I.

V. EXPERIMENTAL IMAGES AND COMPARISON OF SIGNAL AND NOISE LEVELS

Experimental bolometric images for two plasmas are shown in Figs. 4 and 5 for comparison with the synthetic image signal levels. The first (Fig. 4) is for a plasma with C as the only intrinsic impurity and a radiated power of 158 kW to nearly match the SOLPS case. The second image (Fig. 5) is for a plasma with Kr puffing and a much higher radiated power of 1.075 MW. The maximum value of the signal, the experimentally determined error, and the resulting SNR are shown in Table I.

Even though the number of IR camera pixels was quadrupled in order to quadruple the number of bolometer pixels and improve the spatial resolution of the tomographic inversion, reduction in the IR camera frame rate (the bolometer frame rate remained the same) and reduction of the aperture area by

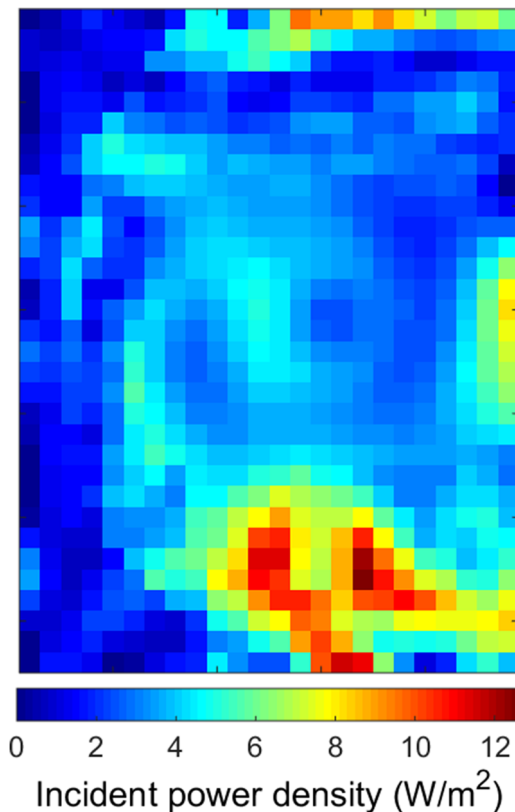


FIG. 4. Bolometric image of radiated power density absorbed by the foil for KSTAR shot 18335, $t = 5.23$ s with intrinsic C impurity.

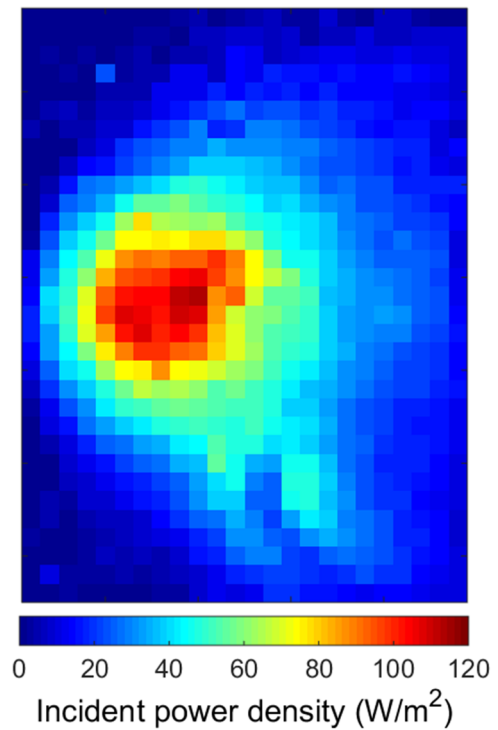


FIG. 5. Bolometric image of radiated power density absorbed by the foil for KSTAR shot 16950, $t = 8.49$ s with puffed Kr impurity.

a factor of two resulted in a reduction of the SNR by a factor of 4 according to the rough signal estimation. The synthetic images from the SOLPS model show a factor of 2 increase in the signal compared to the rough estimate which gives a marginal value of SNR of 10.7. The comparable experimental image shows similar noise and slightly increased signal levels for a SNR of 14.1. Strongly radiating plasmas due to Kr injection show much higher signal levels and a corresponding SNR of 55.

Several anomalies appear in the comparison of the experimental and synthetic images that warrant further investigation. In the data of Fig. 4, anomalously high signal levels are seen at the upper and inboard (right hand side of the image) sides of the images. These have no analogs in the synthetic images and may be due to edge effects at the low signal levels. Also the location of the divertor radiation is significantly different in the synthetic and experimental images. Also in the synthetic image, radiation from the lower left-hand side of the image indicates that something may be wrong with the projection matrix calculation.

VI. CONCLUSIONS AND DISCUSSION

This work has shown that the IRVB on KSTAR could be upgraded to quadruple the number of bolometer pixels while still maintaining reasonable SNR even at the low radiation levels predicted by the SOLPS model. In the 2018 experimental campaign, the power input to the plasma will be increased by the addition of neutral beam power. Therefore, in the future, we expect to have sufficient SNR even for low density plasma with only C impurity.

Differences between the experimental and synthetic images may be due to various assumptions regarding the impurity model, the calculation of the projection matrix, or the location of the IRVB. Therefore, close consideration should be given to all of these assumptions in the future.

ACKNOWLEDGMENTS

This work was supported by the NIFS/NINS Grant No. NIFS16ULHH026 and the NIFS/NINS Japan-Korea Collaboration Grant No. NIFS17KEKO001.

- ¹G. F. Matthews *et al.*, *Phys. Scr.* **T170**, 014035 (2017).
- ²J. Rapp *et al.*, *Nucl. Fusion* **44**, 312 (2004).
- ³H. Meister *et al.*, *Fusion Eng. Des.* **120**, 21 (2017).
- ⁴M. L. Reinke *et al.*, "Experimental tests of an infrared video bolometer on Alcator C-Mod," *Rev. Sci. Instrum.* (to be published).
- ⁵H. Meister *et al.*, *Fusion Eng. Des.* **112**, 579 (2016).
- ⁶A. Huber *et al.*, *Fusion Eng. Des.* **82**, 1327 (2007).
- ⁷B. J. Peterson, *Rev. Sci. Instrum.* **71**, 3696 (2000).
- ⁸B. J. Peterson *et al.*, *Rev. Sci. Instrum.* **74**, 2040 (2003).
- ⁹B. J. Peterson *et al.*, *Rev. Sci. Instrum.* **79**, 10E301 (2008).
- ¹⁰R. Sano *et al.*, *Rev. Sci. Instrum.* **88**, 053506 (2017).
- ¹¹J. Jang *et al.*, *Curr. Appl. Phys.* **18**, 461 (2018).
- ¹²B. J. Peterson *et al.*, *Plasma Fusion Res.* **11**, 2402101 (2016).
- ¹³B. J. Peterson *et al.*, *Rev. Sci. Instrum.* **87**, 11D410 (2016).
- ¹⁴S. Wiesen *et al.*, *J. Nucl. Mater.* **463**, 480 (2015).